NeuroImage: Clinical 11 (2016) 648–657

Contents lists available at ScienceDirect

NeuroImage: Clinical

journal homepage: www.elsevier.com/locate/ynicl

Cerebral metabolism and perfusion in MR-negative individuals with refractory focal epilepsy assessed by simultaneous acquisition of ^{18}F-FDG PET and arterial spin labeling

Ilaria Boscolo Galazzo[a,*], Maria Vittoria Mattoli[b], Francesca Benedetta Pizzini[c], Enrico De Vita[d,e], Anna Barnes[a], John S. Duncan[f], Hans Rolf Jäger[g], Xavier Golay[d,e], Jamshed B. Bomanji[a], Matthias Koepp[f], Ashley M. Groves[a], Francesco Fraioli[a]

[a] Institute of Nuclear Medicine, University College London, London, UK
[b] Institute of Nuclear Medicine, Catholic University of the Sacred Heart, Rome, Italy
[c] Neuroradiology Unit, Department of Diagnostic and Pathology, University Hospital Verona, Verona, Italy
[d] Lysholm Department of Neuroradiology, National Hospital for Neurology and Neurosurgery, London, UK
[e] Department of Brain Repair and Rehabilitation, UCL Institute of Neurology, London, UK
[f] Department of Clinical and Experimental Epilepsy, UCL Institute of Neurology, London, UK
[g] Department of Radiology, University College London Hospitals, London, UK

ARTICLE INFO

Article history:
Received 5 February 2016
Received in revised form 24 March 2016
Accepted 8 April 2016
Available online 12 April 2016

Keywords:
Epilepsy
Arterial spin labeling
Positron emission tomography
Simultaneous PET/MR
Glucose
Cerebral blood flow

ABSTRACT

The major challenge in pre-surgical epileptic patient evaluation is the correct identification of the seizure onset area, especially in MR-negative patients. In this study, we aimed to: (1) assess the concordance between perfusion, from ASL, and metabolism, from ^{18}F-FDG, acquired simultaneously on PET/MR; (2) verify the utility of a statistical approach as supportive diagnostic tool for clinical readers. Secondarily, we compared ^{18}F-FDG PET data from the hybrid PET/MR system with those acquired with PET/CT, with the purpose of validate the reliability of ^{18}F-FDG PET/MR data.

Twenty patients with refractory focal epilepsy, negative MR and a defined electro-clinical diagnosis underwent PET/MR, immediately followed by PET/CT. Standardized uptake value ratio (SUVr) and cerebral blood flow (CBF) maps were calculated for PET/CT-PET/MR and ASL, respectively. For all techniques, *z*-score of the asymmetry index (z_{AI}) was applied for depicting significant Right/Left differences. SUVr and CBF images were firstly visually assessed by two neuroimaging readers, who then re-assessed them considering z_{AI} for reaching a final diagnosis.

High agreement between ^{18}F-FDG PET/MR and ASL was found, showing hypometabolism and hypoperfusion in the same hemisphere in 18/20 patients, while the remaining were normal. They were completely concordant in 14/18, concordant in at least one lobe in the remaining. z_{AI} maps improved readers' confidence in 12/20 and 15/20 patients for ^{18}F-FDG PET/MR and ASL, respectively. ^{18}F-FDG PET/CT-PET/MR showed high agreement, especially when z_{AI} was considered.

The simultaneous metabolism-perfusion acquisition provides excellent concordance on focus lateralisation and good concordance on localisation, determining useful complementary information.

1. Introduction

Epilepsy is the most frequent serious chronic neurological condition (Sander, 2003), and despite advancements in antiepileptic drug therapy, one-third of patients remain poorly controlled on drug treatment. In patients suffering from focal seizures, surgical operation aiming to remove the seizure onset zone (SOZ) may represent the only available option for becoming seizure-free. If an abnormality can be detected on structural magnetic resonance imaging (MR), and is concordant in localisation with the electro-clinical diagnosis, there is usually a 2/3 chance of achieving seizure freedom (Wiebe et al., 2001). However, the odds for seizure freedom are less good if MR is either inconclusive or doesn't reveal structural brain lesions (De Tisi et al., 2011).

In these patients, intracranial EEG recording (iEEG) remains the "gold standard" diagnostic procedure for localising the SOZ and planning surgical resection. Subdural or depth electrodes have to be precisely positioned and limited to specific brain region, in order to minimize

* Corresponding author at: Institute of Nuclear Medicine, University College London, Level 5 UCH, 235 Euston Road, London NW1 2BU, UK.
E-mail addresses: i.galazzo@ucl.ac.uk, ilaria.boscologalazzo@univr.it (I. Boscolo Galazzo).

http://dx.doi.org/10.1016/j.nicl.2016.04.005

risk of surgical complications and achieve the best outcome. Thus, the neurosurgeon requires a reliable diagnostic hypothesis about the localisation of epileptic focus aided by complementary information from different examinations before performing any invasive procedure or even resection of brain tissue appearing normal on MR (Rheims et al., 2013). In this context, functional neuroimaging techniques can provide additional and supportive information about the localisation of the SOZ and may lead to more targeted iEEG investigations if deemed necessary (Brodbeck et al., 2010).

Indeed, the electric changes occurring in the SOZ are often associated with alterations of perfusion and metabolism around the areas of seizure onset and spread. Perfusion single photon emission computed tomography (SPECT) has been successfully employed since the 1980s to assess regional cerebral blood flow (CBF) changes related to the presumed focus, showing ictal hyperperfusion or interictal hypoperfusion (Weil et al., 2001; Calcagni et al., 2002). In light of the several limitations of perfusion SPECT studies, the interest in alternative non-invasive MR-based perfusion techniques, such as Arterial Spin Labeling (ASL), has grown over the last years. ASL provides a fully quantitative measure of regional CBF using arterial blood water magnetically labeled by radiofrequency pulses, proximal to the tissue of interest, as an endogenous diffusible tracer (Williams et al., 1992; Detre et al., 1992; Alsop et al., 2015). Despite the high number of ASL sequences currently available and the limited studies in epilepsy patients, ASL did show promising results, elucidating interictal, ictal and post-ictal alterations in epileptic brain and hemispheric hemodynamic asymmetry (Wolf et al., 2001; Lim et al., 2008; Pizzini et al., 2013; Storti et al., 2014; Boscolo Galazzo et al., 2015; Sierra-Marcos et al., 2016).

[^{18}F]-fluoro-deoxy-D-glucose (^{18}F-FDG) positron emission tomography (PET)/computed tomography (CT) is currently considered the leading imaging modality for the presurgical metabolic assessment during the interictal phase for both temporal (Drzezga et al., 1999; Rathore et al., 2014) and extra-temporal lobe epilepsy (Kim et al., 2000; Juhász et al., 2003), showing regional hypometabolism being associated with the presumed focus. Recently, PET/MR systems have been successfully introduced in clinical practice for the simultaneous acquisition of PET and MR (Catana et al., 2010; Fraioli and Punwani, 2014; Zhang et al., 2014; Ding et al., 2014), providing not only directly superimposable functional and morphological data, but also a proper comparison of different modalities under identical conditions, something that might be essential in dynamic pathologies that rapidly change over time, such as epilepsy.

Due to the complexity and variability in the localisation of the epileptic focus, the clinical relevance of different functional alterations needs to be assessed at the individual patient level. Statistical Parametric Mapping [SPM; Wellcome Department of Cognitive Neurology, London, UK] (Friston et al., 1994) and 3D-SSP/Neurostat (Minoshima et al., 1995) are widely used for semi-quantitatively comparing an individual patient to an age-matched normal database, in order to identify areas of statistically altered metabolism or perfusion (Barnes et al., 2000; Kim et al., 2002; Kumar et al., 2010; Archambaud et al., 2013). Nevertheless, unlike ^{18}F-FDG PET/CT, large datasets from normal subjects are not yet available for ^{18}F-FDG PET/MR, precluding the possibility to compare patient data to controls and to provide a statistical evaluation of individual patient data. As an alternative, for quantifying the differences between hemispheres in focal epilepsy some authors have proposed the application of the Asymmetry Index (AI) parameter, usually comparing AI values over the presumed focus and homotopic regions (Leiderman et al., 1992; Duncan et al., 1993; Theodore et al., 1997).

In this study, we investigated the potential role of a hybrid PET/MR system in a well characterized group of patients with refractory focal epilepsy, primarily aiming to: (1) evaluate perfusion, assessed by ASL, and metabolism, assessed by ^{18}F-FDG, also in relation to the electro-clinically defined SOZ; and (2) evaluate the diagnostic usefulness of an individually tailored approach based on the AI calculation for the automatic identification of significant hemispheric asymmetries in each patient.

In addition, since their different photon attenuation correction, we aimed to compare ^{18}F-FDG PET data from the hybrid PET/MR system with those acquired with PET/CT for investigating the reliability of PET/MR and to determine if it yields additional information beyond that of PET/CT, still considered as "gold standard".

2. Materials and methods

2.1. Patients

Twenty consecutive patients with refractory focal epilepsy (10 men, mean age 34 ± 12 years), undergoing presurgical assessment between March 2013 and October 2014, were enrolled in our study.

The inclusion criteria were: (1) drug-resistant focal epilepsy; (2) negative structural high-resolution 3T-MR scans; (3) well-defined electro-clinical localisation of seizure-onset through ictal/interictal electroencephalogram and video-telemetry (VT-EEG).

Exclusion criteria were: abnormalities on structural MR images, contraindications for MR examinations, concomitant presence of other non-epilepsy neurological disorders, and pregnancy. Patients who satisfied the above criteria underwent simultaneous PET/MR examination and, immediately after, a PET/CT scan using the ^{18}F-FDG activity previously injected.

Electro-clinical diagnostic hypothesis was reached by a multidisciplinary team (MDT) of neurologists, neurophysiologists, neuroradiologists, psychologists and psychiatrists based on clinical history, neuropsychological assessment and electrophysiological findings from VT-EEG monitoring.

The study was approved by the Northeast-Newcastle and North Tyneside 1 Research Ethics Committee and carried out in accordance with the Declaration of Helsinki of the World Medical Association. All patients gave informed consent prior to entering the study.

Patient demographics and clinical characteristics are reported in Table 1.

2.2. PET/MR and ^{18}F-FDG PET/CT acquisition

All patients, fasted for at least 6 h and with the serum glucose level below 7 mmol/l, rested in a dark quiet room and were injected with a bolus of ^{18}F-FDG (range activity 221–292 MBq). 30 min after injection, patients were placed into the PET/MR scanner (Biograph mMR, Siemens Healthcare, Erlangen, Germany) and immobilized with the head coil and specifically designed minimally attenuating pads.

PET/MR protocol started with the acquisition of ultra-short echo time (UTE) sequences in order to calculate a μ-map for attenuation correction [echo times (TE) TE_1: 0.07 ms; TE_2: 2.46 ms; repetition time (TR): 11.9 ms, flip angle: 10°, slice thickness: 1.6 mm; scan duration: 1:40 min] (Dickson et al., 2014; Burgos et al., 2014). At an average time of 35 ± 4 min after ^{18}F-FDG injection, a 3D-brain ^{18}F-FDG PET scan was acquired in list mode [voxel size: 1.40 × 1.40 × 2.03 mm^3; reconstruction: 3 iterations, 21 subsets, 3D Gaussian filter (3.5 mm FWHM); scan duration: 15 min]. During PET data acquisition, ASL data were collected simultaneously. The manufacturer's pulsed PICORE (proximal inversion with a control for off-resonance effects) ASL sequence with Q2TIPS scheme (QUIPSS II with Thin-slice TI1 Periodic Saturation) and 2D-echo planar imaging readout was used [voxel size: 3.6 × 3.6 × 5 mm^3; gap: 1 mm; 19 slices; TI_1/TIs/TI_2: 800/1200/1800 ms; TR/TE: 2860/17 ms; 201 volumes; total acquisition time: 9:36 min]. Standard MR sequences [T2-weighted image, 3D T1-weighted MPRAGE, 2D FLAIR (coronal and axial planes)] were also acquired as part of the PET/MR clinical epilepsy protocol.

Following PET/MR, all patients underwent PET/CT examination with the smallest possible temporal delay. ^{18}F-FDG PET/CT data were acquired on VCT PET/CT systems (GE Healthcare Systems, Waukesha, WI) at an average time of 101.1 min (range 65–140 min) after injection. Patients were immobilized with a head restraint using straps and a

Table 1
Clinical profile: gender, age, seizures characteristics, antiepileptic therapy, and electro-clinical diagnosis from the multi-disciplinary team (MDT) established on the basis of clinical information and electrophysiological findings.

Pt n°	Sex	Age	Years since beginning	Type of seizures	Seizures frequency	Relevant history	Current antiepileptic therapy	MDT
1	F	30	20	Complex partial	12/month	Negative	CBZ, LEV	Right temporal
2	F	28	25	Complex partial	4–6/day	Negative	LTG, PG, PRP	Right temporo-parietal
3	F	40	20	Simple partial with SG	7/month; 1/year (SG)	Febrile convulsion	CBZ, PG	Right temporal
4	F	44	30	Complex partial SG	3–20/month; 1/year (SG)	Meningitis	LEV	Right temporal
5	M	23	3	Simple partial	1–2/week	Febrile convulsion	ESL	Right parietal
6	M	39	14	Simple partial with SG	1–2/week; rare (SG)	Negative	LTG, LEV, RTG	Left fronto-temporal
7	F	39	18	Simple partial with SG	1–5/daily; rare (SG)	Negative	OCX, CLZ, PHE	Left fronto-temporal
8	M	22	6	Complex partial with SG	6–8/month; 1–3/month (SG)	Negative	ZNS, LEV, CLZ	Left temporo-parietal
9	M	19	15	Simple partial with SG	1–2/week; 1–2/month (SG)	Negative	CLZ, OCX, LEV	Right fronto-temporal
10	F	33	17	Complex partial	1–2/week	Negative	LTG, ZNS	Left temporo-occipital
11	F	19	5	Complex partial with SG	4–5/day; 2–3/week (SG)	Negative	LTG, LEV, ZNS, OCX	Left frontal
12	M	23	14	Complex partial	1/day	Negative	VPA, ESL, TPM, LEV	Left frontal
13	M	23	19	Simple partial	2–3/night	Negative	ZNS, LEV, CLZ	Right frontal
14	M	65	16	Complex partial	1/day	Negative	VPA, LTG	Left temporal
15	F	41	17	Complex partial	2–3/day	Negative	ZNS, ESL, CLZ	Right temporal
16	M	31	15	Simple partial with SG	2/month; rare (SG)	Negative	LEV, LCM	Right temporal
17	M	38	8	Complex partial with SG	1–2/month; rare (SG)	Negative	OCX. CLZ, ZNS, VPA	Left temporal
18	F	55	49	Complex partial	2–3/week	Negative	VPA, CBZ, CLZ, ZNS	Right fronto-temporal
19	F	39	30	Complex partial	Several/week	Negative	OCX, TPM, CLP, CLZ	Left temporal
20	M	40	7	Complex partial	3/week	Negative	CBZ, LTG	Right temporal

SG = secondary generalization; CBZ = carbamazepine; LEV = levetiracetam; LTG = lamotrigine; PG = pregabilin; PRP = parampanel; ESL = eslicarbazepine; RTG = retigabine; OCX = oxocarbazepine;CLZ = clobazam; PHE = phenytoin; ZNS = zonisamide; VPA = valproate; TPM = topiramate; LCM = lacosamide; CLP = clonazepam.

3D-brain ^{18}F-FDG PET scan was acquired in list mode [voxel size: $1.95 \times 1.95 \times 3.27$ mm^3; reconstruction: 3 iterations, 20 subsets, 3D Hanning filter (cut-off 4 mm); scan duration: 15 min]. Additionally, for attenuation and scatter correction, an unenhanced low-dose CT scan (140 kVp, 80 mA, 0.8 s, pitch 1.75/1.375) was obtained.

2.3. ASL and PET data analysis

ASL data were preprocessed and analyzed using FSL 5.0.1 (FMRIB, Oxford, UK) and Matlab 7.14 (MathWorks, Natick, MA) with a dedicated in-house code developed for this study. Motion correction was applied separately to the Control and Label volumes using the MCFLIRT tool in FSL and taking the first volume as reference. In particular, a six-parameter 3D rigid-body registration with a normalized correlation cost function was used. The first volume, which represents the ASL calibration scan, was also used for estimating the coregistration parameters from ASL to the individual T1-weighted image by applying a 3D rigid-body registration with a normalized mutual-information cost function and 7 degrees of freedom. After computing the mean Control-Label over the multiple repetitions, quantification of CBF maps was performed according to the recently published guidelines (Alsop et al., 2015). CBF maps in ASL space were affine-registered to the individual high-resolution anatomical images by applying the previously estimated transformation matrix. Each T1-weighted image was then registered to the MNI (Montreal Neurological Institute) space with $1 \times 1 \times 1$ mm^3 resolution using a non-linear method (FNIRT tool in FSL). Finally, the joint ASL/T1-weighted and T1-weighted/MNI space transformation parameters were used to spatially normalize the CBF maps, which were then smoothed with a 2 mm FWHM Gaussian kernel.

^{18}F-FDG data acquired with PET/CT and PET/MR were corrected for photon attenuation and registered to individual high-resolution anatomical images, using normalized mutual information as the cost function and 7 degrees of freedom. The joint PET/T1-weighted and T1-weighted/MNI space transformation parameters were used to spatially normalize the PET data. PET data in MNI space were transformed into maps representing the standardized uptake value ratio (SUVr) which is defined as the tissue concentration of radioactivity (kBq/ml) in each voxel normalized to the mean activity concentration in a reference region, here represented by the cerebellum. In particular, a gray matter (GM) cerebellum mask was manually delineated on the spatially normalized individual T1-weighted image and then applied to PET data in the same space to calculate the mean activity concentration in the reference region.

2.4. Evaluation of metabolic/perfusion abnormalities with the asymmetry index

The normalization of ASL and ^{18}F-FDG PET datasets to the same standard coordinate space allowed a voxelwise comparison between modalities as well as identification of Left/Right asymmetries in the cerebral hemispheres and the cortical lobes. Assuming the epileptic focus was located in one hemisphere, as our population of patients with focal seizures was well-selected, a significant difference in metabolism/perfusion between the abnormal area and the corresponding location in the opposite hemisphere would be expected.

Therefore, in order to identify the voxels potentially corresponding to the epileptic focus we defined for both CBF and SUVr maps of each patient a voxelwise AI as:

$$AI = 100 * [Right - Left]/[(Right + Left)/2]. \quad (1)$$

This was calculated for every voxel in the Right hemisphere, with positive values indicating Right > Left and negative values Right < Left (Lim et al., 2008; Duncan et al., 1993; Theodore et al., 1997).

After calculating the mean (μ_{AI}) and standard deviation (SD_{AI}) of the whole set of AI values, a voxelwise AI z-score map (z_{AI}) was derived as:

$$z_{AI} = \frac{value_{AI} - \mu_{AI}}{SD_{AI}}. \quad (2)$$

Assuming a normal distribution of values, voxels with $|z_{AI}| \geq 1.64$ corresponding to $p < 0.05$ were considered to have significantly different SUVr or CBF between hemispheres. For visualization purposes, brain voxels with statistically significant asymmetric metabolism/perfusion were displayed on the Right hemisphere if $z_{AI} \leq -1.64$ (Right < Left) and on the Left hemisphere if $z_{AI} \geq 1.64$ (Right > Left).

2.5. Clinical interpretation of ^{18}F-FDG PET/CT, ^{18}F-FDG PET/MR and ASL data

Two imaging specialists with several years' experience in neuroradiology and nuclear medicine (F.F., 10 years; F.B.P., 11 years), unaware of clinical data, visually evaluated the normalized ^{18}F-FDG PET/CT, ^{18}F-FDG PET/MR and ASL images in the same way a week apart, in order to

identify metabolic and perfusion abnormalities. They were first asked to grade the level of overall scan as normal, or abnormal. Second, readers were instructed to report more extensive details on brain metabolism/perfusion, encompassing the main involved brain lobes (i.e., frontal, temporal, parietal, occipital), in order to lateralise and localize the altered patterns, if present.

Afterwards, the two readers re-examined the images taking into account the corresponding z_{AI} maps showing clusters of significant hemispheric asymmetries. Based on these statistical results and the original images, the final report regarding lateralisation/localisation of the presumed epileptic focus was made (visual + z_{AI}). Any disagreement between the two readers was resolved by consulting a third senior neuroradiologist/nuclear medicine physician.

2.6. Comparison between ^{18}F-FDG PET/CT and ^{18}F-FDG PET/MR findings

The visual assessment and the final decision (visual + z_{AI}) of ^{18}F-FDG PET/CT and PET/MR from the two readers in consensus were compared in each patient. Moreover, the level of agreement between the two modalities for each of the two reports (visual and visual + z_{AI}) was quantified by a Kappa test defined as:

$$K = (Po - Pe)/(1 - Pe) \quad (3)$$

where Po = observed proportional agreement, Pe = random proportional agreement. Interpretation of the level of agreement was as follows: 0.0–0.2 slight; 0.2–0.4 fair; 0.4–0.6 moderate; 0.6–0.8 substantial; 0.8–1.0 almost perfect (Richard Landis and Koch, 1977).

Regarding image quantification results, Pearson's correlation coefficient (r) was calculated for each patient between all the AI values from the two modalities, in order to compare on a voxel-by-voxel basis the degree of hemispheric asymmetry estimated with the two techniques. Further, the z_{AI} values of the voxels classified as having significantly different SUVr between hemispheres for ^{18}F-FDG PET-CT and PET-MR were compared using an unpaired t-test, with statistical significance determined as $p < 0.05$. The mean and standard deviation of these z_{AI} values over the statistical threshold were also calculated in each patient.

To specify regional correlations across patients, the SUVr maps from ^{18}F-FDG PET/CT and PET/MR were compared within ten regions of interest (ROIs) based on the Harvard-Oxford atlases and commonly assessed in neurological studies: the hippocampus, cerebellum, insula, thalamus, frontal lobes, temporal lobes, occipital lobes, parietal lobes, striata and precuneus. In particular, the mean SUVr values for ^{18}F-FDG PET/CT and PET/MR were extracted from the ten ROIs in each patient, which were correlated across the twenty subjects using Pearson's correlation coefficients (r). Further, the mean SUVr values of the ten ROIs were compared using paired t-test ($p < 0.05$).

All these preliminary analyses were focused on a more technical and direct comparison of ^{18}F-FDG PET data acquired with two different systems, in order to assess the reliability of ^{18}F-FDG PET/MR, independently from the diagnosis of epilepsy, and considering ^{18}F-FDG PET/CT as “gold standard”.

2.7. Comparison between ^{18}F-FDG PET/MR and ASL findings

After the preliminary direct comparison between ^{18}F-FDG PET/CT and PET/MR data, all subsequent analyses were focused on ^{18}F-FDG PET/MR and ASL data simultaneously acquired with the PET/MR scanner. For these imaging modalities, besides the two consensus reports (visual and visual + z_{AI}), the impact of the statistical z_{AI} maps on the confidence of imaging reporting was also noted in order to quantify the effectiveness of this method as a decision aid. In particular, the readers' confidence after the presentation of the z_{AI} maps was assigned to one of the following categories: Unchanged and Improved.

The final decisions for ^{18}F-FDG PET/MR and ASL data (visual + z_{AI}) were qualitatively compared in order to evaluate the concordance between changes in metabolism and perfusion in each epileptic patient. The level of agreement between the final decisions coming from the two modalities was also quantified using the Kappa test as previously described (Eq. (3)).

Subsequently, ^{18}F-FDG PET/MR and ASL imaging results were statistically compared in terms of cross-subject regional correlations within the ten ROIs as defined in the previous paragraph. In particular, for ASL the CBF maps of each patient were voxel-wise intensity normalized to the mean CBF in the same cerebellum mask as for the ^{18}F-FDG PET/MR data, in order to generate relative CBF maps (rCBF) which were more suitable for the inter-modality statistical comparison. Thus, the mean rCBF and SUVr values were extracted from the different ROIs, which were then correlated across the twenty patients using Spearman's rank correlation coefficients (r_s value). Further, the mean rCBF and SUVr values in the same brain regions were statistically compared using a Wilcoxon signed-rank test ($p < 0.05$).

2.8. Comparison of electro-clinical diagnostic hypothesis with ^{18}F-FDG PET/MR and ASL

For each modality separately, the level of agreement between each of the two consensus reports (visual and visual + z_{AI}) and the electro-clinical diagnosis established by MDT was assessed using the Kappa test as described by Eq.(3), which also allowed to indirectly quantify the usefulness of the z_{AI} method.

The overall information provided by the combination of ^{18}F-FDG PET/MR and ASL results, considered as a unique technique, was also qualitative compared to the electro-clinical MDT diagnosis to assess the performance of the simultaneous multimodal approach.

3. Results

All patients completed the full investigative protocol: none of them reported any seizure onset, i.e. all patients were evaluated during the interictal phase, and no irregular major movements were detected during the acquisitions.

Clinical information and MDT electro-clinical diagnosis of the epileptic focus are summarized in Table 1. Figs. 1 and 2 present imaging results from a selection of 12 representative patients (6 with a presumed Right hemisphere epileptic focus and 6 with a presumed Left hemisphere epileptic focus), showing the semiquantitative SUVr maps for PET data and the quantitative CBF maps for ASL, along with the corresponding z_{AI}.

The main ^{18}F-FDG PET/CT, ^{18}F-FDG PET/MR and ASL results are summarized in Tables 2 to 4. In particular, Table 2 includes the results from the statistical analyses between ^{18}F-FDG PET/CT-PET/MR across all the patients, while in the Supplementary material Table 1 the main imaging and statistical findings for these two techniques are reported on an individual basis. Finally, imaging and statistical comparisons between ^{18}F-FDG PET/MR and ASL are summarized in Tables 3 and 4.

3.1. Comparison between ^{18}F-FDG PET/CT and ^{18}F-FDG PET/MR findings

Visually, ^{18}F-FDG PET/CT and ^{18}F-FDG PET/MR showed hypometabolism in the same 17/20 patients, and both were normal in the remaining (Supplementary Table 1). In particular, ^{18}F-FDG PET/CT and ^{18}F-FDG PET/MR were concordant in lateralising abnormalities to the same side in 17/17 patients and in localising to the same lobe in 15/17 patients. In the remaining 2 patients (#8 and #14) ^{18}F-FDG PET/MR and ^{18}F-FDG PET/CT were partially concordant, with at least one common region identified.

Accounting for ^{18}F-FDG z_{AI} statistical maps, ^{18}F-FDG PET/CT and ^{18}F-FDG PET/MR showed hypometabolism concordant for lateralisation and localisation in the same 17 patients plus a further patient (#4) who was visually classified as normal. Thus, ^{18}F-FDG PET/CT and ^{18}F-FDG PET/MR

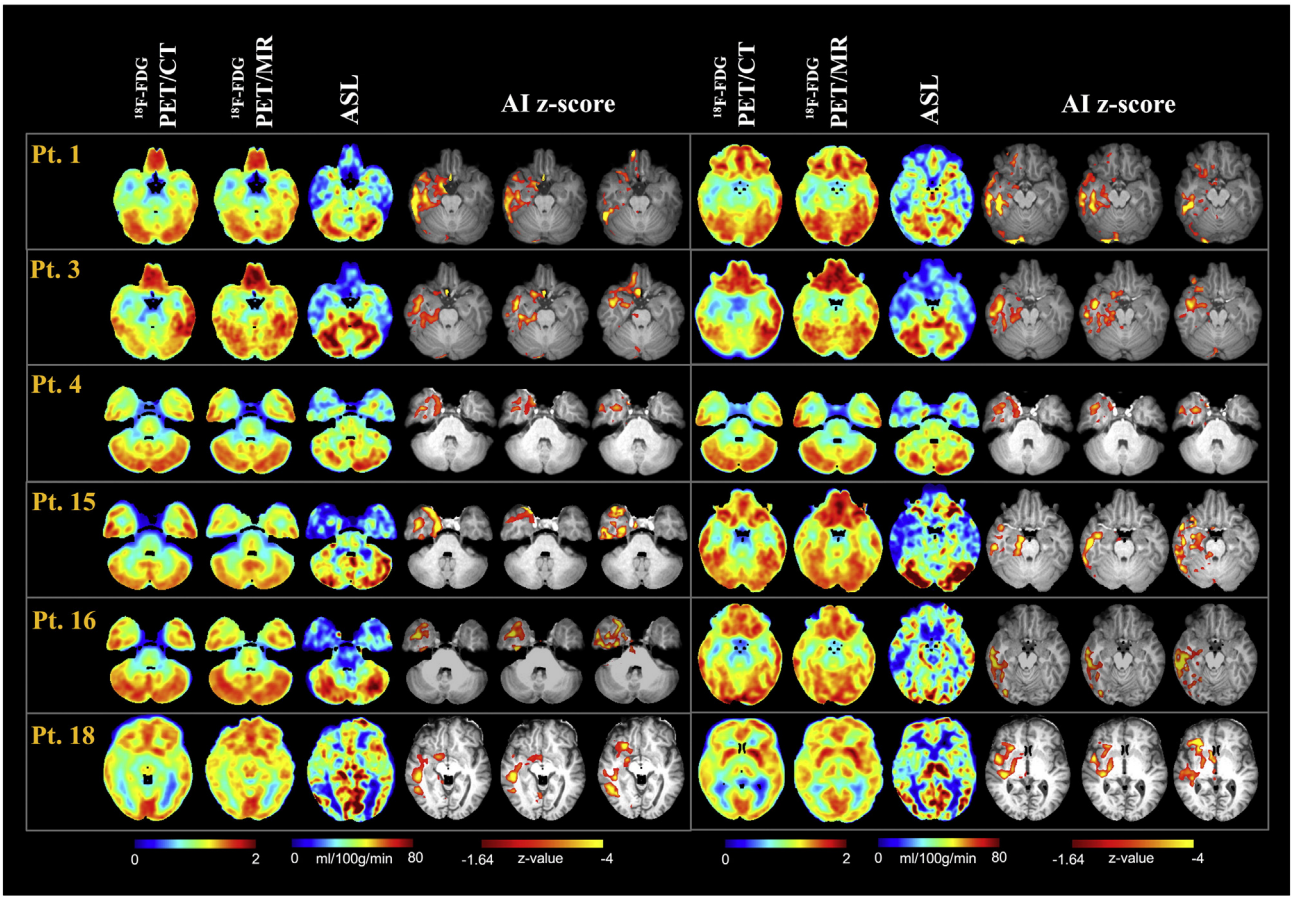

Fig. 1. ^{18}F-FDG PET/CT, ^{18}F-FDG PET/MR, ASL and the corresponding z_{AI} statistical maps for some representative patients with a Right hemisphere focal localisation (normalized data). SUVr and CBF maps for two slices of interest encompassing the presumed focus are reported for ^{18}F-FDG PET and ASL, respectively.

were completely concordant in all the 18 patients with metabolic alterations (Supplementary Table 1). The statistical Kappa test confirmed an almost perfect agreement between ^{18}F-FDG PET/CT and ^{18}F-FDG PET/MR results for visual assessment (K = 0.845), and perfect agreement (K = 1) for the visual + z_{AI} report.

Voxel-by-voxel comparison between the AI values of ^{18}F-FDG PET/CT and of ^{18}F-FDG PET/MR showed significant correlation in all cases, with $p < 0.0005$ in each patient, and an overall mean correlation coefficient of $r = 0.91 \pm 0.05$ (Supplementary Table 1). Moreover, considering only voxels with statistical significant z_{AI} values, no statistically significant differences were found between ^{18}F-FDG PET/CT and ^{18}F-FDG PET/MR z_{AI} values ($p > 0.05$).

Scatter plots of the mean SUVr values from ^{18}F-FDG PET/CT and ^{18}F-FDG PET/MR in a series of ROIs are presented in Fig. 3A. The overall correlation across twenty patients in the ten ROIs was strong ($r = 0.85$, $p < 0.0005$), with all the ROIs showing significant results ($p < 0.0005$) and Pearson's correlation coefficients over $r = 0.68$ (Table 2). When testing the differences between the mean ^{18}F-FDG PET/CT and ^{18}F-FDG PET/MR SUVr values, 4 ROIs (occipital and parietal lobes, thalamus, hippocampus) showed a statistically significant difference (Table 2).

3.2. Comparison between ^{18}F-FDG PET/MR and ASL findings

Visually, ^{18}F-FDG PET/MR showed hypometabolism in 17/20 patients, while in the remaining 3 patients ^{18}F-FDG PET/MR did not show any marked metabolic abnormality (Table 3, Figs. 1 and 2). After consultation of ^{18}F-FDG z_{AI} maps, the readers identified hypometabolic areas in one additional patient, while in the remaining 2 patients (#2 and #5), no statistical significant asymmetries were identified on the z_{AI} maps and thus remained classified as normal. The addition of ^{18}F-FDG z_{AI} maps to the visual assessment improved the readers' confidence in image reporting in 12/20 patients. In particular, in patients #4 and #8 the information from the z_{AI} maps allowed to highly increase the readers' confidence, which changed their final decision when reassessed the imaging maps.

Visually, ASL images showed hypoperfusion in 17/20 patients, while in the remaining 3 patients ASL did not show any marked perfusion abnormality (Table 3, Figs. 1 and 2). After consultation of ASL z_{AI} maps, the readers identified hypoperfused areas in one additional patient, while in the remaining 2 (#2 and #5) no statistical significant asymmetries were identified on the z_{AI} maps and thus remained classified as normal. The ASL z_{AI} maps improved the readers' confidence in 15/20 patients, in particular in patients #4 and #7 they led to a change in the final diagnosis when reassessing the CBF maps.

Comparing the two modalities' findings and focusing on the final decision (visual + z_{AI} report) performed by the two readers, ^{18}F-FDG PET/MR and ASL both showed functional changes in 18/20 patients, while they were both normal in the remaining. In the 18 patients with focally reduced perfusion and metabolism, the two techniques were concordant regarding lateralisation in all 18/18 patients, and regarding localisation in 14/18 patients. We observed partial concordance in the remaining 4 patients, showing coexistence of metabolism-perfusion coupled/uncoupled patterns (Table 3). The statistical Kappa test confirmed a substantial agreement in final decision between ^{18}F-FDG PET/MR and ASL results (K = 0.723).

Scatter plots of the mean SUVr and rCBF values from ^{18}F-FDG PET/MR and ASL in a series of ROIs are presented in Fig. 3B. The overall correlation across twenty patients in the ten ROIs was good ($r_s = 0.49$, $p < 0.0005$), with significant Spearman correlation coefficients for 5 ROIs (frontal, temporal and parietal lobes, striata and hippocampus). Conversely, low

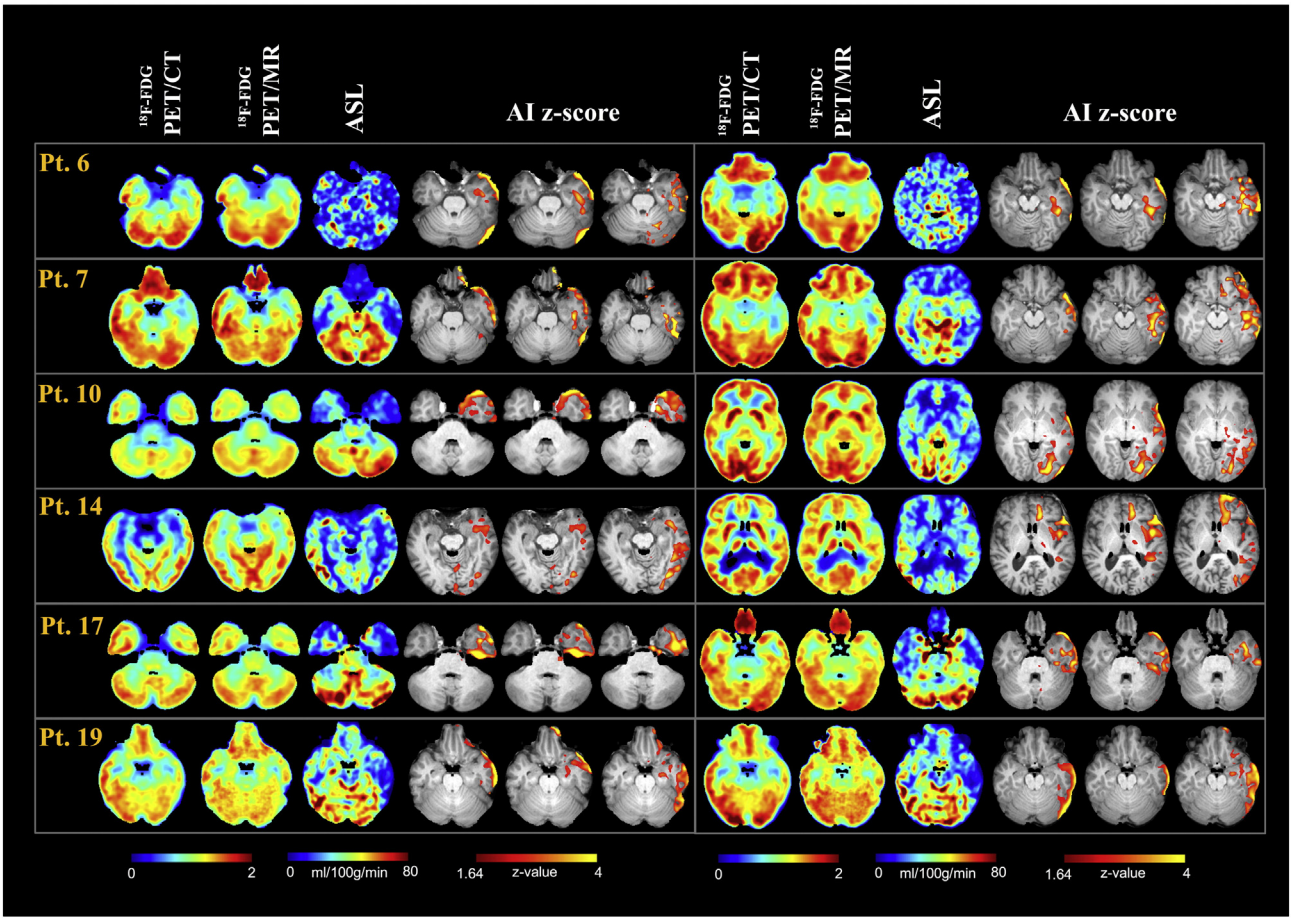

Fig. 2. ^{18}F-FDG PET/CT, ^{18}F-FDG PET/MR, ASL and the corresponding z_{AI} statistical maps for some representative patients with a Left hemisphere focal localisation (normalized data). SUVr and CBF maps for two slices of interest encompassing the presumed focus are reported for ^{18}F-FDG PET and ASL, respectively.

correlations were found in the insula and cerebellum. When testing the differences between the mean SUVr and rCBF values, 5 ROIs (occipital and parietal lobes, striata, thalamus, precuneus) showed a statistically significant difference (Table 4).

3.3. Comparison of electro-clinical diagnostic hypothesis with ^{18}F-FDG PET/MR and ASL

Regarding the localisation of epileptic focus, the hypometabolic areas visually identified by ^{18}F-FDG PET/MR were in agreement with electro-clinical MDT diagnosis in 13/20 patients. After ^{18}F-FDG z_{AI} maps consultation, areas of hypometabolism were concordant with MDT in 15/20 patients (Table 3). These findings were confirmed by statistical Kappa test that showed a moderate agreement between visual ^{18}F-FDG PET/MR and MDT (K = 0.514), substantially improved by the consultation of the z_{AI} maps (K = 0.650).

For ASL, the areas of hypoperfusion visually identified on the CBF maps concurred with the electro-clinical data in 11/20 patients. After ASL z_{AI} maps consultation, ASL was concordant in a further 2 patients (#4 and #7, Table 3). The statistical kappa test showed a moderate agreement between ASL visually assessed and MDT (K = 0.406), that became stronger after the consultation of z_{AI} maps (K = 0.532).

In regards to the combined complementary information provided by ^{18}F-FDG and ASL, there was a perfect agreement in lateralisation and localisation among ^{18}F-FDG, ASL and MDT in 12/20 patients; in one case (patient #7), the combination of ^{18}F-FDG and ASL allowed to reach a perfect agreement with the electro-clinical diagnosis. In one further patient (#6), while the electro-clinical diagnosis was widespread, the combination of ^{18}F-FDG and ASL showed a more focal area of functional alteration. Conversely, in 4/20 patients a reverse pattern was seen, with the combination of ^{18}F-FDG and ASL showing a more widespread area of functional alterations in comparison to MDT (Table 3).

Table 2
Cross subject Pearson's r correlation (column 1) and *t*-test results (column 2 and 3) between SUVr of ^{18}F-FDG PET/CT and SUVr of ^{18}F-FDG PET/MR in 10 regions of interest.

Region of interest	Correlation	*t*-value	*p*-Value
Frontal	0.85	2.01	0.051
Temporal	0.89	1.48	0.147
Occipital	0.68	2.53	0.015
Parietal	0.72	2.30	0.027
Cerebellum	0.94	0.63	0.530
Striata	0.83	−1.34	0.195
Thalamus	0.82	−4.18	0.002
Hippocampus	0.80	−6.24	0.000
Insula	0.93	−0.26	0.935
Precuneus	0.80	1.10	0.280

p-Value for Pearson's r correlation coefficient was <0.0005 in each region

4. Discussion

We report the first simultaneously acquired investigation of the relationship between metabolic and perfusion data using a hybrid PET/MR scanner in patients with refractory focal epilepsy. In this group of difficult-to-treat patients with negative structural MR, ^{18}F-FDG PET/MR and ASL were able to identify regions of metabolic and perfusion abnormality in the majority of the patients, showing complete agreement in lateralising seizure onset, a complete agreement in localising seizure onset area in 14/20 patients and partial concordance with at least one

Table 3
^{18}F-FDG PET/MR and ASL results: visual assessment, final decision after z_{AI} consultation (visual + z_{AI}) and readers' confidence in their decision after image reassessment with z_{AI} information. The electro-clinical diagnosis about focus localisation from the multi-disciplinary team (MDT) is also reported.

Pt n°	MDT	^{18}F-FDG PET/MR visual	^{18}F-FDG PET/MR visual + z_{AI}	Readers' confidence after z_{AI} maps	ASL visual	ASL visual + z_{AI}	Readers' confidence after z_{AI} maps
1	Right temporal	Right temporal	Right temporal	Unchanged	Right temporal	Right temporal	Unchanged
2	Right temporo-parietal	Normal	Normal	–	Normal	Normal	–
3	Right temporal	Right temporal	Right temporal	Improved	Right temporal	Right temporal	Improved
4	Right temporal	Normal	Right temporal	Improved (*)	Normal	Right temporal	Improved (*)
5	Right parietal	Normal	Normal	–	Normal	Normal	–
6	Left fronto-temporal	Left temporal	Left temporal	Unchanged	Left temporal	Left temporal	Unchanged
7	Left fronto-temporal	Left temporal	Left temporal	Improved	Left temporal	Left fronto-temporal	Improved (*)
8	Left temporo-parietal	Left temporal	Left temporo-parietal	Improved (*)	Left fronto-parietal	Left fronto-parietal	Improved
9	Right fronto-temporal	Right fronto-temporal	Right Fronto-Temporal	Improved	Right fronto-temporal	Right fronto-temporal	Improved
10	Left temporo-occipital	Left temporo-occipital	Left temporo-occipital	Unchanged	Left temporo-occipital	Left temporo-occipital	Improved
11	Left frontal	Left frontal	Left frontal	Unchanged	Left fronto-parietal	Left fronto-parietal	Improved
12	Left frontal	Left frontal	Left frontal	Unchanged	Left fronto-parietal	Left fronto-parietal	Improved
13	Right frontal	Right frontal	Right frontal	Unchanged	Right frontal	Right frontal	Unchanged
14	Left temporal	Left fronto-temporal	Left fronto-temporal	Improved	Left fronto-temporal	Left fronto-temporal	Improved
15	Right temporal	Right temporal	Right temporal	Improved	Right temporal	Right temporal	Improved
16	Right temporal	Right temporal	Right temporal	Improved	Right temporal	Right temporal	Improved
17	Left temporal	Left temporal	Left temporal	Improved	Left temporal	Left temporal	Improved
18	Right fronto-temporal	Right fronto-temporal	Right fronto-temporal	Improved	Right fronto-temporal	Right fronto-temporal	Improved
19	Left temporal	Left temporal	Left temporal	Improved	Left temporal	Left temporal	Improved
20	Right temporal	Right temporal	Right temporal	Improved	Right temporal	Right temporal	Improved

(*) Readers confidence has been highly improved by the z_{AI} consultation (i.e. they changed their initial judgment)

common lobe identified in a further four patients. Furthermore, these non-invasive techniques provided concordant and, in some cases, complementary information which allowed confirmation of the electro-clinical diagnosis formulated by a multi-disciplinary panel that integrates seizure semiology, long-term VT-EEG and structural neuroimaging, using clinical experience. In the management of these patients, it is of great importance to have reliable diagnostic imaging tools that would be able to confirm and add confidence in the clinical diagnostic hypothesis, helping the clinician and neurosurgeon in the selection of the best therapeutic approach.

In our study, we primarily investigated whether ^{18}F-FDG PET and ASL data, simultaneously acquired with a hybrid PET/MR system, were able to identify regional abnormalities possibly related to the epileptic focus, and if metabolism and perfusion alterations were effectively coupled in the interictal period. In the last years, multiparametric functional imaging modalities became essential tools in the diagnostic evaluation of epilepsy although, in everyday clinical practice, the acquisition of functional parameters is mainly undertaken separately at different times, leading to a possible bias in the epileptic focus localization. The possibility given by the recent PET/MR scanners of simultaneous functional acquisitions (such as metabolism with ^{18}F-FDG PET and perfusion with ASL MR) can allow a proper comparison between them, as the acquisitions occur under the same physiological or pathophysiological conditions. The advantages of this simultaneous acquisition are extremely helpful in epilepsy, which is probably one of the field that could gain more from PET/MR acquisitions as the events under study in this pathology, such as spikes and spikes-waves, are often paroxysms that might change rapidly over time. With the hybrid system, the epileptic patient can be evaluated under identical conditions, being sure that any physiological or pathological event is "captured" by each imaging technique at the same moment. Although areas of hypoperfusion and hypometabolism cannot be expected to perfectly overlap, due to different technical and physiological parameters as well as different underlying mechanisms (Leybaert, 2005), we found perfusion/metabolism coupling in the majority (16/20) of our patients, whereas the area of hypometabolism was more circumscribed than the hypoperfusion area in the remaining. Previous studies also reported the presence of uncoupled metabolism/perfusion pattern in drug-resistant epilepsy (Gaillard et al., 1995), although in many cases there was a larger hypometabolic area than hypoperfusion area (Bouilleret et al., 2002). The simultaneous evaluation of both parameters indicates the vascular bed is impaired while the metabolism is still preserved suggesting that flow alterations might precede metabolic changes. Moreover, the larger areas of perfusion alterations might indicate not only the region of seizure origin but also the seizure propagation pathways, suggesting the presence of a complex altered network. When statistically compared, data showed an overall good correlation between rCBF, as measured by ASL, and SUVr, as measured by ^{18}F-FDG PET/MR, with presence of regional variability and the highest correlations between the mean rCBF and SUVr values across patients in frontal and temporal lobes. Our results are in agreement with previous published data (Cha et al., 2013) correlating cerebral perfusion from ASL and glucose metabolism from ^{18}F-FDG PET/CT acquired in separate sessions in normal volunteers. They showed that, despite an overall good correlation between perfusion and metabolism in healthy controls, there was considerable regional variability with seemingly 'uncoupled' perfusion and metabolism in medial structures which may exist as a normal phenomenon or may be attributed to technical and acquisition parameters.

An important point of clinical relevance is that our study further demonstrates the feasibility of ASL as an important presurgical epilepsy tool. ^{18}F-FDG PET, looking for a focal area of hypometabolism during the interictal phase, is a well-established method for the presurgical epilepsy evaluation in clinical practice, especially if structural MR is negative or is discordant with the clinical hypothesis. Conversely, despite the promising results recently shown in literature (Storti et al., 2014; Blauwblomme et al., 2014; Boscolo Galazzo et al., 2015; Sierra-Marcos et al., 2016), the application of ASL for epileptic patients' evaluation in clinical practice is still limited. Here, we aimed to further demonstrate its reliability and applicability (using the manufacturer's ASL sequence,

Table 4
Cross subject Spearman's r_s correlation (column 1 and 2) and Wilcoxon signed-ranks test results (column 3 and 4) between SUVr and rCBF values in 10 regions of interest.

Region of interest	Correlation	*p*-Value	Wilcoxon test	*p*-Value
Frontal	0.64	0.021	−1.87	0.080
Temporal	0.58	0.042	−1.42	0.128
Occipital	0.49	0.101	−2.55	0.011
Parietal	0.54	0.049	−3.04	0.002
Cerebellum	0.28	0.353	−1.93	0.057
Striata	0.59	0.040	−2.90	0.004
Thalamus	0.27	0.363	−2.69	0.007
Hippocampus	0.55	0.045	−1.57	0.120
Insula	0.21	0.475	−1.55	0.120
Precuneus	0.46	0.115	−2.76	0.006

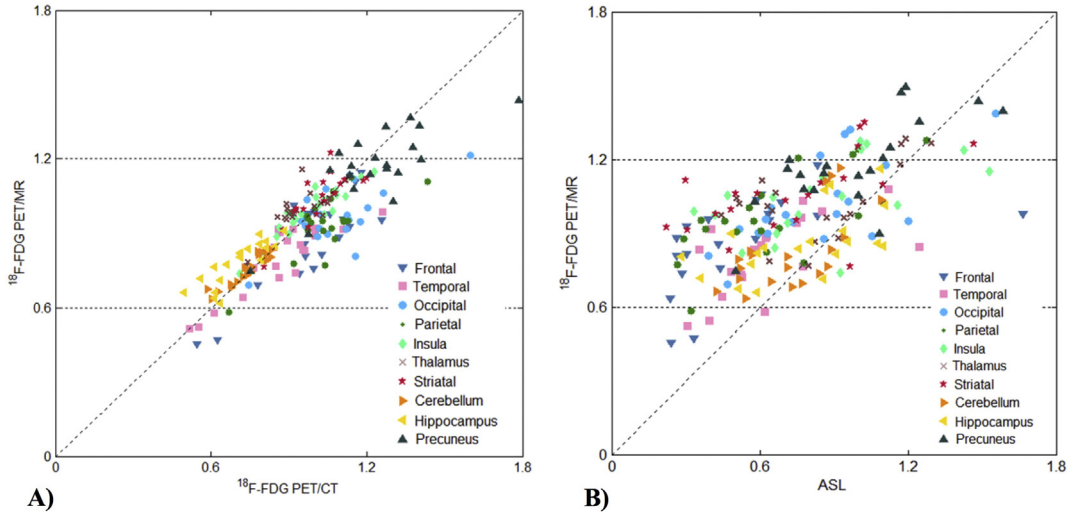

Fig. 3. Regional comparison across the twenty patients for ten regions of interest. A) ^{18}F-FDG PET/CT vs ^{18}F-FDG PET/MR; B) ASL vs ^{18}F-FDG PET/MR.

carefully optimised for the study) as a possible alternative to nuclear medicine techniques in some cases or a complementary method to derive a more complete picture of the pathological changes. Indeed, the good concordance between ^{18}F-FDG PET and ASL results shown in our group of patients indicates that it is viable to apply ASL, looking for focal hypoperfusion during the interictal phase, instead of using ^{18}F-FDG PET, which may not be available in all centres, or for limiting its application, as it exposes the patient to radiations. Thus, there is a marked ASL potential in the presurgical work up of patients who have normal MR (or MR findings that are discordant from electro-clinical diagnostic hypothesis) in helping to localize the epileptic focus, as shown by our results.

In this study, besides assessing the information provided by the two neuroimaging techniques, we also addressed the more technical and clinically important problem of analyzing individual patient data. Indeed, in the case of epilepsy, group analyses are often precluded and each patient has to be singularly evaluated to identify the possible areas of functional alterations related to the epileptic focus. In this field, computer-aided diagnosis tools are increasingly relied upon in order to more reliably interpret brain images and to obtain objective and observer-independent information for each patient, allowing an increase in the specialist's confidence in image reporting. However, all the main tools that have been successfully applied to deal with these problems, even in clinical settings, like SPM, 3D-SSP/Neurostat, Scenium (Siemens AG, New York, NY) and Cortex ID (GE Healthcare), involve the statistical comparison to a reference age-matched control group, data that however is not yet widely available nor easy to acquire for ^{18}F-FDG PET/MR. Here we propose an alternative method to identify at patient level the areas of statistically significant changes without using the information derived from a normal database and we demonstrate its usefulness as a reliable statistical analysis tool to support the visual image interpretation performed by clinical readers. This is mainly based on the voxelwise calculation of metabolism/perfusion asymmetries between the two hemispheres, a parameter (AI) that has already been successfully applied in previous papers (Wolf et al., 2001; Duncan et al., 1993; Theodore et al., 1997) and is clinically relevant to detect focal abnormalities in this patient population. Previous studies using the AI index generally compared the estimated AI values to a reference threshold derived from a normal population to identify the significant voxels (Leiderman et al., 1992; Ding et al., 2014) or only qualitative evaluated the asymmetries between specific regions over the presumed epileptic focus (Wolf et al., 2001), without providing statistical significance to the results. In our case, since no control group were available for any of the three modalities, we overcame this limitation applying an individually-tailored *z*-score test to the estimated AI values, using the information estimated from each patient to automatically identify areas with statistically significant asymmetries. This tool enhanced readers' initial visual judgment, improving their confidence in the majority of patients or streamlining more restricted brain areas for a more precise assessment of functional changes that are often difficult to be clearly localized, especially in the case of ASL. Indeed, mainly due to the low signal-to-noise ratio of ASL and its high sensitivity to motion artefacts, CBF maps might be difficult to assess visually, especially if the reader has limited experience with this relative new technique. Therefore, the interpretation of ASL results at patient level as well as those coming from ^{18}F-FDG PET can take advantage of the support of a statistical analysis tool such as the AI *z*-scores. The information provided by z_{AI} maps resulted in a change of the final decision in > 10% of patients for both ^{18}F-FDG PET/MR and ASL, resulting in the two modalities becoming concordant with the electro-clinical diagnosis in all cases. In particular, patient #4 had metabolism and perfusion visually considered unremarkable, but z_{AI} maps showed overlapping regions of metabolic and perfusion abnormality that allowed a revised final diagnosis which was concordant with the electro-clinical diagnosis. Our consistent results across the modalities suggest that, even in absence of a comparable normal database derived by healthy volunteers, z_{AI} is a valid supportive tool for readers reporting different imaging studies of individuals with well-lateralised disease, such as focal epilepsy.

Regarding the concordance with the electro-clinical MDT diagnosis, ^{18}F-FDG PET/MR and ASL final decisions were fully concordant with MDT in lateralisation in all patients. For the localisation, ^{18}F-FDG PET/MR was in better agreement with the clinical hypothesis than ASL (15 vs 13). However, the perfect concordance between several modalities achieved in 13/18 patients increases the confidence in focus localisation in MR-negative epileptic patients, improving preparation for intracranial electrode implantations if deemed necessary (Brodbeck et al., 2010) and, in selected cases, possibly leading to resective surgery without further invasive recording.

As secondary aim, we also focused on the qualitative and quantitative comparison between the ^{18}F-FDG PET component of PET/CT and PET/MR, evaluating the effects of the different photon attenuation correction used in the two hybrid devices. Although the advantages in simultaneous acquisition of PET and MR data are numerous, the major challenge with this new system is the lack of an optimal MR sequence to clearly measure the bone information, as in the case of CT systems, in order to have an accurate correction of PET photon attenuation. This aspect is particularly important in the brain, which is completely surrounded by bone and where quantitative assessment of PET data may be affected (Dickson et al., 2014; Burgos et al., 2014). In our study we used the UTE sequence for the MR-based attenuation correction, which has been shown to lead to significant improvements in the

accuracy of PET uptake measurements in the brain, being able to capture bone information (Keereman et al., 2010). Looking at the ^{18}F-FDG activity concentration, we found in all patients a consistent underestimation for ^{18}F-FDG PET/MR in comparison to ^{18}F-FDG PET/CT in most of the cortical areas [results not shown], in agreement with several previous brain studies involving ^{18}F-FDG PET/MR (Dickson et al., 2014; Al-Nabhani et al., 2014). However, when we calculated SUVr maps for both modalities and statistically compared the results, we found significant correlations between SUVr values of PET/CT and PET/MR in each ROI and an overall high Pearson's correlation coefficient across all the ROIs of the twenty patients. Only few regions showed a significant difference in the mean SUVr values between the two modalities. Our results are in line previous studies having the same aim (Catana et al., 2010; Berker et al., 2012; Dickson et al., 2014), which all reflect an overestimation of SUVr PET/MR in hippocampus and subcortical areas, such as thalamus, and an underestimation in other cortical areas, as occipital lobe, when compared with SUVr PET/CT, which is considered the reference standard for attenuation correction. However, these elements and differences did not impact onto the clinical interpretations of data. We found an excellent overall agreement between the clinical evaluations of ^{18}F-FDG PET/CT and ^{18}F-FDG PET/MR images performed by the two readers in consensus, which was almost perfect for visual evaluation and perfect for final decision (visual + z_{AI}), as shown by the Kappa test. Moreover, the two modalities have highly correlated AI maps and lead to similar z_{AI} statistical maps, both in terms of values and distribution, further confirming the good agreement between them. Thus, despite the different PET activity, the information provided by the two modalities was highly correlated and the local metabolic alterations well measured with ^{18}F-FDG PET/MR.

Although we proved that simultaneous ^{18}F-FDG PET/MR is a feasible technique to study individuals with focal refractory epilepsy, we recognise some limitations. Firstly, in this difficult to control group of patients with normal MR scans, we lack a gold-standard in most of the cases, who have not yet gone for surgery, and no histopathological confirmation or outcome data are available. We have to rely on the diagnostic hypothesis reached by a consensus panel and based on uncertainties derived from clinical and electrophysiological data such as seizure semiology, neuropsychology and long-term VT-EEG. Although most of the patients included in the present study are now awaiting further invasive EEG recording, only one of our patients had undergone the surgical procedure, confirming the SOZ suggested by PET/MR. However, the good concordance between the electro-clinical data and the functional imaging data fore-assured the clinicians, leading now to the planning of invasive tests for the majority of the patients. Secondarily, the sample of this study is small, as we restricted the selection to the group of MR-negative patients but well-defined clinical diagnostic hypothesis about lateralisation. More studies on larger, less selected groups are necessary to further evaluate the performance of each modality and to better assess the added value of a multimodal simultaneous imaging approach.

5. Conclusion

This is the first study to our knowledge that combines a simultaneous multimodality approach to evaluate cerebral perfusion with glucose metabolism in a well-selected patient population with MR-negative refractory focal epilepsy. The AI *z*-score is a valuable and useful statistical analysis tool that increases the confidence of the neuroimaging reader, especially for ASL data. Even supported by this automated-aided tool, the simultaneous acquisition of metabolism and perfusion provides excellent concordance on lateralisation and good concordance on localisation of epileptic focus. Furthermore, the imaging findings from PET/MR concurred with the electro-clinical hypothesis in the majority of patients, providing concordant and complementary information useful for the management of this difficult-to-treat population. Therefore, in the absence of a non-invasive gold standard, multimodality imaging allows for a more comprehensive evaluation and can contribute to a better assessment of the epileptogenic focus.

Conflict of interest

The authors declare no conflict of interest.

The following are the supplementary data related to this article.

Supplementary data to this article can be found online at http://dx.doi.org/10.1016/j.nicl.2016.04.005.

Acknowledgements

The authors thank Dr. John C. Dickson, Prof. Peter Ell and Prof. Maria Lucia Calcagni for their supportive comments. We also want to thank Robert Shortman, Celia O'Meara and all the Nuclear Medicine staff for their help with patient's recruitment, contribution to the clinical investigation and tireless work. Authors are also grateful to Dr. Afshin Nasoodi for his contribution with the collection of data.

The collaboration with Verona was facilitated by the COST Action BM1103 on "Arterial Spin Labeling in Dementia (AID)".

This work was taken at UCLH/UCL which received a proportion of funding from the Department of Health's NIHR Biomedical Centres (BRC UCLH 2012) funding scheme.

References

Al-Nabhani, K.Z., Syed, R., Michopoulou, S., Alkalbani, J., Afaq, A., Panagiotidis, E., et al., 2014. Qualitative and quantitative comparison of PET/CT and PET/MR imaging in clinical practice. J. Nucl. Med. 55, 88–94.

Alsop, D.C., Detre, J.A., Golay, X., Günther, M., Hendrikse, J., Hernandez-Garcia, L., et al., 2015. Recommended implementation of arterial spin-labeled perfusion MRI for clinical applications: a consensus of the ISMRM perfusion study group and the European consortium for ASL in dementia. Magn. Reson. Med. 73, 102–116.

Archambaud, F., Bouilleret, V., Hertz-Pannier, L., Chaumet-Riffaud, P., Rodrigo, S., Dulac, O., et al., 2013. Optimizing statistical parametric mapping analysis of 18F-FDG PET in children. EJNMMI Res. 3, 2.

Barnes, A., Lusman, D., Patterson, J., Brown, D., Wyper, D., 2000. The use of statistical parametric mapping (SPM96) as a decision aid in the differential diagnosis of dementia using 99mTc-HMPAO SPECT. Behav. Neurol. 12, 77–86.

Berker, Y., Franke, J., Salomon, A., Palmowski, M., Donker, H.C., Temur, Y., et al., 2012. MRI-based attenuation correction for hybrid PET/MRI systems: a 4-class tissue segmentation technique using a combined ultrashort-echo-time/Dixon MRI sequence. J. Nucl. Med. 53, 796–804.

Blauwblomme, T., Boddaert, N., Chémaly, N., Chiron, C., Pages, M., Varlet, P., et al., 2014. Arterial spin labeling MRI: a step forward in non-invasive delineation of focal cortical dysplasia in children. Epilepsy Res. 108, 1932–1939.

Boscolo Galazzo, I., Storti, S.F., Del Felice, A., Pizzini, F.B., Arcaro, C., Formaggio, E., et al., 2015. Patient-specific detection of cerebral blood flow alterations as assessed by arterial spin labeling in drug-resistant epileptic patients. PLoS One 10, e0123975.

Bouilleret, V., Valenti, M.P., Hirsch, E., Semah, F., Namer, I.J., 2002. Correlation between PET and SISCOM in temporal lobe epilepsy. J. Nucl. Med. 43, 991–998.

Brodbeck, V., Spinelli, L., Lascano, A.M., Pollo, C., Schaller, K., et al., 2010. Electrical source imaging for presurgical focus localisation in epilepsy patients with normal MRI. Epilepsia 51, 583–591.

Burgos, N., Cardoso, M.J., Thielemans, K., Modat, M., Pedemonte, S., Dickson, J., et al., 2014. Attenuation correction synthesis for hybrid PET-MR scanners: application to brain studies. IEEE Trans. Med. Imaging 33, 2332–2341.

Calcagni, M.L., Giordano, A., Bruno, I., Parbonetti, G., Di Giuda, D., De Rossi, G., et al., 2002. Ictal brain SPET during seizures pharmacologically provoked with pentylenetetrazol: a new diagnostic procedure in drug-resistant epileptic patients. Eur. J. Nucl. Med. Mol. Imaging 29, 1298–1306.

Catana, C., van der Kouwe, A., Benner, T., Michel, C.J., Hamm, M., Fenchel, M., et al., 2010. Toward implementing an MRI-based PET attenuation-correction method for neurologic studies on the MR-PET brain prototype. J. Nucl. Med. 51, 1431–1438.

Cha, Y.H., Jog, M.A., Kim, Y.C., Chakrapani, S., Kraman, S.M., Wang, D.J., 2013. Regional correlation between resting state FDG PET and pCASL perfusion MRI. J. Cereb. Blood Flow Metab. 33, 1909–1914.

De Tisi, J., Bell, G.S., Peacock, J.L., Aw, McEvoy, Harkness, W.F.J., Sander, J.W., et al., 2011. The long-term outcome of adult epilepsy surgery, patterns of seizure remission and relapse: a cohort study. Lancet 378, 1388–1395.

Detre, J.A., Leigh, J.S., Williams, D.S., Koretsky, A.P., 1992. Perfusion imaging. Magn. Reson. Med. 23, 37–45.

Dickson, J.C., O'Meara, C., Barnes, A., 2014. A comparison of CT- and MR-based attenuation correction in neurological PET. Eur. J. Nucl. Med. Mol. Imaging 41, 1176–1189.

Ding, Y.S., Chen, B.B., Glielmi, B., Friedman, K., Devinsky, O., 2014. A pilot study in epilepsy patients using simultaneous PET/MR. Am. J. Nucl. Med. Mol. Imaging 4, 459–470.

Drzezga, A., Arnold, S., Minoshima, S., Noachtar, S., Szecsi, J., Winkler, P., et al., 1999. 18F-FDG PET studies in patients with extratemporal and temporal epilepsy: evaluation of an observer-independent analysis. J. Nucl. Med. 40, 737–746.

Duncan, R., Patterson, J., Roberts, R., Hadley, D.M., Bone, I., 1993. Ictal/postictal SPECT in the presurgical localisation of complex partial seizures. J. Neurol. Neurosurg. Psychiatry 56, 141–148.

Fraioli, F., Punwani, S., 2014. Clinical and research applications of simultaneous positron emission tomography and MRI. Br. J. Radiol. 87, 20130464.

Friston, K.J., Holmes, A.P., Worsley, K.J., Poline, J.P., Frith, C.D., Frackowiak, S.J., 1994. Statistical parametric maps in functional imaging: a general linear approach. Hum. Brain Mapp. 2, 189–210.

Gaillard, W.D., Fazilat, S., White, S., Malow, B., Sato, S., Reeves, P., et al., 1995. Interictal metabolism and blood flow are uncoupled in temporal lobe cortex of patients with complex partial epilepsy. Neurology 45, 1841–1847.

Juhász, C., Chugani, D.C., Muzik, O., Shah, A., Asano, E., Mangner, T.J., et al., 2003. Alpha-methyl-L-tryptophan PET detects epileptogenic cortex in children with intractable epilepsy. Neurology 60, 960–968.

Keereman, V., Fierens, Y., Broux, T., Deene, Y.D., Lonneux, M., Vandenberghe, S., 2010. MRI-based attenuation correction for PET/MRI using ultrashort echo time sequences. J. Nucl. Med. 51, 812–818.

Kim, S.K., Wang, K.C., Hwang, Y.S., Kim, K.J., Kim, I.O., Lee, D.S., et al., 2000. Pediatric intractable epilepsy: the role of presurgical evaluation and seizure outcome. Childs Nerv. Syst. 16, 278–285.

Kim, Y.K., Lee, D.S., Lee, S.K., Chung, C.K., Chung, J.K., Lee, M.C., 2002. (18)F-FDG PET in localisation of frontal lobe epilepsy: comparison of visual and SPM analysis. J. Nucl. Med. 43, 1167–1174.

Kumar, A., Juhasz, C., Asano, E., Sood, S., Muzik, O., Chugani, H.T., 2010. Objective detection of epileptic foci by 18F-FDG PET in children undergoing epilepsy surgery. J. Nucl. Med. 51, 1901–1907.

Leiderman, D.B., Balish, M., Sato, S., Kufta, C., Reeves, P., Gaillard, W.D., et al., 1992. Comparison of PET measurements of cerebral blood flow and glucose metabolism for the localisation of human epileptic foci. Epilepsy Res. 13, 153–157.

Leybaert, L., 2005. Neurobarrier coupling in the brain: a partner of neurovascular and neurometabolic coupling? J. Cereb. Blood Flow Metab. 25, 2–16.

Lim, Y.M., Cho, Y.W., Shamim, S., Solomon, J., Birn, R., et al., 2008. Usefulness of pulsed arterial spin labeling MR imaging in mesialtemporal lobe epilepsy. Epilepsy Res. 82, 183–189.

Minoshima, S., Frey, K.A., Koeppe, R.A., Foster, N.L., Kuhl, D.E., 1995. A diagnostic approach in Alzheimer's disease using three-dimensional stereotactic surface projections of fluorine-18-FDG PET. J. Nucl. Med. 36, 1238–1248.

Pizzini, F.B., Farace, P., Manganotti, P., Zoccatelli, G., Bongiovanni, L.G., Golay, X., et al., 2013. Cerebral perfusion alterations in epileptic patients during peri-ictal and post-ictal phase: PASL vs DSC-MRI. Magn. Reson. Imaging 31, 1001–1005.

Rathore, C., Dickson, J.C., Teotónio, R., Ell, P., Duncan, J.S., 2014. The utility of 18F-fluorodeoxyglucose PET (FDG PET) in epilepsy surgery. Epilepsy Res. 108, 1306–1314.

Rheims, S., Jung, J., Ryvlin, P., 2013. Combination of PET and magnetoencephalography in the presurgical assessment of MRI-negative epilepsy. Front. Neurol. 4, 188.

Richard Landis, J., Koch, G.G., 1977. The measurement of observer agreement for categorical data. Biometrics 33, 159–174.

Sander, J.W., 2003. The epidemiology of epilepsy revisited. Curr. Opin. Neurol. 16, 165–170.

Sierra-Marcos, A., Carreño, M., Setoain, X., López-Rueda, A., Aparicio, J., Donaire, A., et al., 2016. Accuracy of arterial spin labeling magnetic resonance imaging (MRI) perfusion in detecting the epileptogenic zone in patients with drug-resistant neocortical epilepsy: comparison with electrophysiological data, structural MRI, SISCOM and FDG-PET. Eur. J. Neurol. 23, 160–167.

Storti, S.F., Boscolo Galazzo, I., Del Felice, A., Pizzini, F.B., Arcaro, C., et al., 2014. Combining ESI, ASL and PET for quantitative assessment of drug-resistant focal epilepsy. NeuroImage 102, 49–59.

Theodore, W.H., Sato, S., Kufta, C.V., Gaillard, W.D., Kelley, K., 1997. FDG-positron emission tomography and invasive EEG: seizure focus detection and surgical outcome. Epilepsia 38, 81–86.

Weil, S., Noachtar, S., Arnold, S., Yousry, T.A., Winkler, P.A., Tatsch, K., 2001. Ictal ECD-SPECT differentiates between temporal and extratemporal epilepsy: confirmation by excellent postoperative seizure control. Nucl. Med. Commun. 22, 233–237.

Wiebe, S., Blume, W.T., Girvin, J.P., Eliasziw, M., 2001. A randomized, controlled trial of surgery for temporal-lobe epilepsy. N. Engl. J. Med. 345, 311–318.

Williams, D.S., Detre, J.A., Leigh, J.S., Koretsky, A.P., 1992. Magnetic resonance imaging of perfusion using spin inversion of arterial water. Proc. Natl. Acad. Sci. U. S. A. 89, 212–216.

Wolf, R.L., Alsop, D.C., Levy-Reis, I., Meyer, P.T., Maldjian, J.A., Gonzalez-Atavales, J., et al., 2001. Detection of mesial temporal lobe hypoperfusion in patients with temporal lobe epilepsy by use of arterial spin labeled perfusion MR imaging. AJNR Am. J. Neuroradiol. 22, 1334–1341.

Zhang, K., Herzog, H., Mauler, J., Filss, C., Okell, T.W., Kops, E.R., et al., 2014. Comparison of cerebral blood flow acquired by simultaneous [15O] water positron emission tomography and arterial spin labeling magnetic resonance imaging. J. Cereb. Blood Flow Metab. 34, 1373–1380.